

HYDRA: HYBRID DEEP MAGNETIC RESONANCE FINGERPRINTING

Pingfan Song* Yonina C. Eldar[#] Gal Mazor[#] Miguel R. D. Rodrigues*

* Department of Electronic and Electrical Engineering, University College London, UK

[#] Department of Electrical Engineering, Technion – Israel Institute of Technology, Israel

ABSTRACT

Magnetic resonance fingerprinting (MRF) methods typically rely on dictionary matching to map the temporal MRF signals to quantitative tissue parameters. Such approaches suffer from inherent discretization errors, as well as high computational complexity as the dictionary size grows. To alleviate these issues, we propose a HYbrid Deep magnetic Resonance fingerprinting approach, referred to as HYDRA, which involves two stages: a model-based signature restoration phase and a learning-based parameter restoration phase. The former phase is implemented using low-rank based de-aliasing techniques and the latter phase is implemented using a deep residual convolutional neural network (MRF-ResNet). The designed network is trained on synthesized MRF data simulated with the Bloch equations and fast imaging with steady state precession (FISP) sequences, and then it takes a temporal MRF signal as input and produces the corresponding tissue parameters. In contrast to conventional dictionary-matching-based MRF approaches, our approach significantly improves the inference speed by eliminating the time-consuming dictionary matching operation, and alleviates discretization errors by outputting continuous-valued parameters. We further avoid the need to store a large dictionary. We validated our MRF-ResNet on both synthetic data and phantom data generated from a healthy subject, demonstrating improved performance over state-of-the-art MRF approaches in terms of inference speed, reconstruction accuracy, and storage requirements.

Index Terms— Magnetic Resonance Fingerprinting, Quantitative Magnetic Resonance Imaging, Deep Learning, Residual Convolutional Neural Network

1. INTRODUCTION

Magnetic Resonance Fingerprinting (MRF) [1–6] has emerged as a promising Quantitative Magnetic Resonance Imaging (QMRI) approach, with the capability of providing multiple

tissue’s intrinsic spin parameters simultaneously, such as the spin-lattice magnetic relaxation time (T1) and the spin-spin magnetic relaxation time (T2). Based on the fact that the response from each tissue with respect to a given pseudo-random pulse sequence is unique, MRF exploits pseudo-randomized acquisition parameters to create unique temporal signal signatures, analogous to a "fingerprint", for different tissues. A dictionary matching operation is then performed to map an inquiry temporal signature to the best matching entry in a precomputed dictionary, leading to multiple tissue parameters directly.

The temporal signatures are generated by varying the acquisition parameters of a pseudo-random excitation pulse sequence, such as repetition time (TR), time of echo (TE), and radio frequency flip angle (FA) over time. The dictionary is composed of a large number of entries that are usually simulated by the Bloch equations given pseudo-random pulse sequences. Each entry represents a unique temporal signature associated with a specific tissue and its quantitative parameters, such as the T1 and T2 relaxation times. Thus, once the best matching (i.e. most correlated) entry is found, it directly leads to multiple quantitative parameters simultaneously via a lookup-table operation.

MRI physics and physiological constraints make the MR scanning procedure time-consuming. To shorten the acquisition time, a subsampling operation is commonly performed in the k-space (a.k.a conjugate Fourier transform domain) in order to reduce the number of samples and accelerate imaging speed. However, such k-space subsampling results in temporal signatures that are corrupted by aliasing, blurring and noise. This hampers the accuracy associated with the estimation of the tissue parameters using a dictionary matching procedure. In order to alleviate the impact of such distortion and corruption, de-aliasing operations are often exploited to restore cleaner signatures before performing signature-to-parameter mapping. Therefore, MRF reconstruction usually involves two operations: signature restoration and parameter restoration.

In particular, inspired by the successful application of sparsity-driven image processing approaches in MRI reconstruction [7–9], several works [3–6] suggest to incorporate prior knowledge such as sparsity and low-rank to attenuate distortion and corruption, improving the signature restoration

This work was supported by the Royal Society International Exchange Scheme IE160348, by the European Union’s Horizon 2020 grant ERC-BNYQ, by the Israel Science Foundation grant no. 335/14, by ICore: the Israeli Excellence Center ‘Circle of Light’, by the Ministry of Science and Technology, Israel, by UCL Overseas Research Scholarship (UCL-ORS) and by China Scholarship Council (CSC).

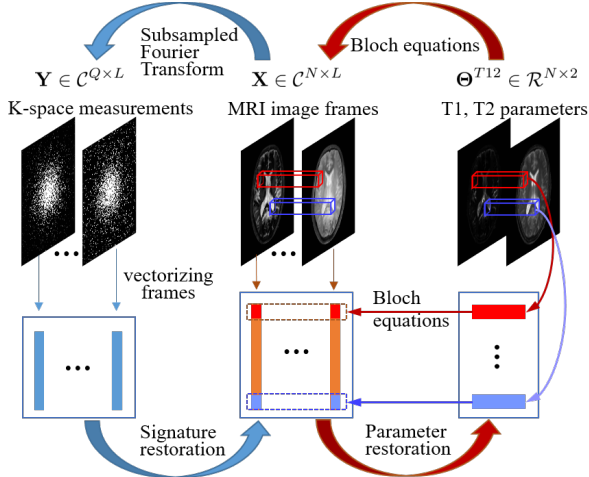


Fig. 1. Relationship between key variables. The MR contrast matrix \mathbf{X} is associated with the k-space measurements \mathbf{Y} per column by the subsampled Fourier transform. It is related to tissue parameters $\Theta^{T_{12}}$ per row by the Bloch equations. Given $\Theta^{T_{RE}}$ and \mathbf{Y} , the image stack \mathbf{X} is commonly first reconstructed from \mathbf{Y} , referred to as signature restoration, and then mapped to tissue parameters $\Theta^{T_{12}}$ via dictionary matching, referred to as parameter restoration.

performance, during the initial MRF reconstruction stage. This is then also followed by a dictionary matching operation, performing mapping from purified temporal signatures to tissue’s quantitative parameters. However, such dictionary matching based signature-to-parameter mapping exhibits several drawbacks [10, 11]. Since the simulated dictionary and lookup-table contain a finite number of elements, they can only cover a limited number of discrete values for each type of tissue parameter. We refer to the difference between a continuous-valued tissue parameter and its closest available discrete value on a lattice as the discretization error. For example, a pair of dictionary and lookup-table that contain 101 elements will lead to a discretization error of maximum 25 ms if they cover the range of 0 ms - 5000 ms with a fixed interval of 50 ms for a specific tissue parameter, e.g. T1. To reduce the discretization error, a huge dictionary that is composed of a large number of entries is needed to represent tissues with fine granularity over the entire value range of target tissue parameters. However, storing a large dictionary becomes prohibitively memory-consuming, as the dictionary size and density often increase exponentially with the number of tissue parameters. In specific, the number of entries in a dictionary will be P^s for s parameters with each containing P values, since every combination of these s parameters determines a specific tissue which is characterized by a specific signature. For example, given T1, T2 relaxations, i.e. $s = 2$, if each of them contains 1000 values, the dictionary will have 1000^2 entries. In addition, finding the best matching entry becomes computationally intense for a large dictionary, considerably limiting the inference speed.

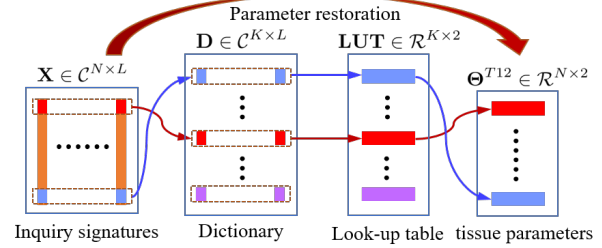


Fig. 2. Parameter restoration using dictionary matching. Given an inquiry temporal signature, dictionary matching computes its inner product with each dictionary entry, and selects the most correlated one with the highest inner product as the best matching signature. Once the best matching entry is found, it directly leads to multiple tissue parameters, such as T1, T2, simultaneously, via searching a lookup-table.

In this paper, we propose an alternative approach to dictionary matching based on deep neural networks (a.k.a. deep learning) [12, 13], which we refer to as HYDRA: HYbrid Deep magnetic Resonance fingerprinting. The motivation derives from the fact that a well designed and tuned deep neural network is capable of approximating complex functions, leading to state-of-the-art results in a number of tasks such as image classification, super-resolution, speech recognition, and more [14–20]. Recent work [10, 11] have proposed to exploit neural networks to replace the dictionary and the lookup-table used in conventional MRF reconstruction approaches. These proposed neural networks based approaches suffer from two limitations: (1) First, these approaches are based on neural network models containing only 3-layers, thus suffer from limited capacity of capturing complex mapping functions. (2) Second, these approaches focused exclusively on the parameter restoration stage (the second stage in MRF reconstruction), but not on the signature restoration one (the first stage in MRF reconstruction). Therefore, these approaches have fully relied on fully-sampled instead of typically available sub-sampled k-space data.

Different from Cohen et al.’s fully-connected feed-forward neural network [10], and Hoppe et al.’s convolutional neural network (CNN) model [11], the proposed HYDRA involves both a signature restoration and a parameter restoration phase, where the signature restoration is implemented using a low-rank based de-aliasing method adapted from [6] and the parameter restoration is implemented using proposed deep residual convolutional neural network, referred to as MRF-ResNet. HYDRA therefore eliminates the requirement for the memory and time-consuming dictionary matching operation, thus significantly improving the inference speed without compromising on the reconstruction performance. In short, the key differences of our approach from other literature includes: (1) HYDRA is, to the best of our knowledge, the first one to combine model-based de-aliasing and learning-based parameter mapping. (2) HYDRA is therefore also able to handle both fully-sampled k-space data, as [10, 11] and more

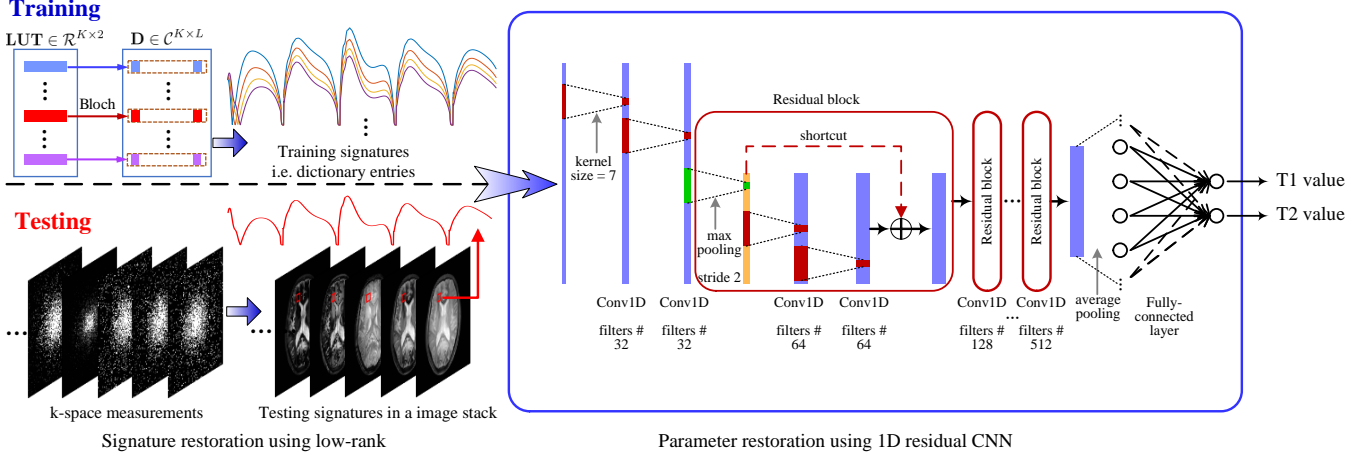


Fig. 3. Diagram of the proposed MRF reconstruction approach. During the training stage, synthesized dictionary entries are used as training signatures to train the proposed 1D residual CNN until the outputs approximate parameter values in LUT well. In this way, the network captures the signature-to-parameter mapping. During the testing stage, a low-rank based algorithm is used to restore the image stack, a matrix containing signatures in rows, from k-space measurements. Then the restored signatures are input into the trained network to obtain corresponding tissue parameters directly. Note, the testing stage does not require the synthesized dictionary and dictionary matching operations, as they are replaced by the trained network.

importantly sub-sampled k-space data. (3) Our MRF-ResNet is deeper than competing network models owing to a residual learning structure. (4) Our approach only uses simulated data for network training, but can still be applied to phantom/real MRF data.

The main contributions of our work include:

- A 1D residual convolutional neural network is designed to capture the mappings from temporal MRF signals to tissue parameters. The designed MRF-ResNet is trained on synthesized MRF data simulated with the Bloch equations, eliminating the requirement for a large amount of real MRF data.
- A low-rank based de-aliasing method is exploited for signature restoration without requiring a dictionary for projection.
- The low-rank based signature restoration is organically combined with the learning-based parameter restoration to achieve fast and accurate MRF reconstruction.
- A series of numerical experiments are conducted to evaluate the proposed approach on both synthetic data and phantom data. The results demonstrate improved inference speed, accuracy and discretization errors over competing methods [1–6, 10, 11].

The rest of the paper is organized as follows. In Section 2, we formulate the MRF reconstruction problem. In Section 3, we introduce related work. Section 4 presents our approach, involving the use of a low-rank based signature restoration procedure together with a learning-based parameter restoration approach. Section 5 is devoted to experiments. We conclude in Section 6.

2. THE MRF PROBLEM FORMULATION

MRF data is composed of multiple frames sampled in k-space over time. A series of such frames are vectorized and then stacked together along the temporal dimension to construct a measurement matrix $\mathbf{Y} \in \mathbb{C}^{Q \times L}$, where Q is the number of k-space samples in each frame, and L is the number of frames, equivalent to the number of time points. Due to k-space sub-sampling, every column vector $\mathbf{Y}_{:,i}$ represents a subsampled Fourier transform of a vectorized image frame $\mathbf{X}_{:,i}$:

$$\mathbf{Y} = [\mathbf{Y}_{:,1}, \dots, \mathbf{Y}_{:,L}] = [F_u\{\mathbf{X}_{:,1}\}, \dots, F_u\{\mathbf{X}_{:,L}\}], \quad (1)$$

where $F_u\{\cdot\}$ denotes a subsampled 2D Fourier transform.

Each column $\mathbf{X}_{:,i}$ represents a MR contrast acquired with RF sequence parameters:

$$\Theta_{:,i}^{TRE} = [TR^i, TE^i, FA^i]^T, \quad i \in [1, L] \quad (2)$$

where TR^i and TE^i denote the repetition time and echo time, respectively, and FA^i denotes the flip angle of the RF pulse at sampling time point i . Every row $\mathbf{X}_{j,:}$ represents a temporal signature, i.e. temporal signal evolution of a specific tissue at the j -th image pixel. The signature depends on the tissue's relaxation times, such as T1 and T2, grouped as a row vector:

$$\Theta_{j,:}^{T12} = [T1^j, T2^j], \quad j \in [1, N] \quad (3)$$

where, N denotes the number of pixels in each image frame. Note that, j is the spatial index while i is the temporal index throughout. Given RF sequence parameters Θ^{TRE} , and parameters $\Theta_{j,:}^{T12}$ of a specific tissue, its temporal signature $\mathbf{X}_{j,:}$ can be derived as:

$$\mathbf{X}_{j,:} = f(\Theta_{j,:}^{T12}, \Theta^{TRE}) \quad (4)$$

where $f(\cdot)$ denotes the Bloch equations. This MR contrast matrix \mathbf{X} is associated with the k-space measurements \mathbf{Y} per column by the subsampled Fourier transform, and it is related to tissue parameters Θ^{T12} per row by the Bloch equations, as illustrated in Fig. 1.

Given RF sequence parameters Θ^{TRE} and k-space measurements \mathbf{Y} , the goal of MRF reconstruction is to estimate the tissue parameters Θ^{T12} . Typically, the image stack \mathbf{X} is first reconstructed from \mathbf{Y} , referred to as signature restoration, and then mapped to tissue parameters Θ^{T12} via dictionary matching, referred to as parameter restoration [1–6], as illustrated in Fig. 2.

The dictionary is a collection of temporal signatures that are usually simulated by the Bloch equations for various typical tissues, given the pseudo-random RF pulse sequences and tissue parameters. Given an inquiry temporal signature, dictionary matching computes the inner product between the temporal signature with each dictionary entry, selecting the entry in the dictionary exhibiting the highest correlation with the inquiry one as the best matching signature. Once the best matching entry is found, it directly leads to multiple tissue parameters, such as T1, T2, simultaneously, via searching a lookup-table.

Let $\mathbf{LUT} \in \mathcal{R}^{K \times 2}$ denote a lookup-table composed of K tissues, each containing 2 parameters, i.e., T1 and T2 relaxation times¹. Let $\mathbf{D} \in \mathcal{C}^{K \times L}$ denote the corresponding dictionary simulated using Bloch equations given the RF sequence parameters Θ^{TRE} , formulated as $\mathbf{D}_{k,:} = f(\mathbf{LUT}_{k,:}, \Theta^{TRE})$. Since each temporal signature $\mathbf{D}_{k,:}$ is linked with the k -th tissue’s parameters $\mathbf{LUT}_{k,:}$, the choice of a large dictionary size K can in principle provide enough granularity to capture a range of possible tissue values.

In conclusion, existing MRF reconstruction approaches involve two stages: signature restoration and parameter restoration, that can be succinctly written as follows

$$\Theta_{j,:}^{T12} = g(h(\mathbf{Y})_{j,:} | \Theta^{TRE}), j \in [1, N], \quad (5)$$

where the function $\mathbf{X} = h(\mathbf{Y})$ represents the signature restoration operation such as sparsity or low-rank based de-aliasing and denoising methods, whereas the function $g(\mathbf{X}_{j,:} | \Theta^{TRE})$ represents the parameter restoration operation, such as dictionary matching based methods [1–6].

Our approach aims to perform signature restoration via low-rank based de-aliasing and parameter restoration via a neural network in order to achieve improved MRF reconstruction performance. We highlight that our approach only requires a simulated dictionary during the network training. Once the network is trained, the dictionary is not needed anymore. In addition, our approach also eliminates a simulated dictionary for signature restoration, which is a key difference

¹Note that the off resonance parameter, which appeared in the original MRF paper [1], has been omitted here, since the sequence used in our experiments is derived from the FISP sequence, which is insensitive to off resonance effects [2, 6].

from FLOR [5,6] during the signature restoration. In sum, we have eliminated the requirement for a simulated dictionary for MRF reconstruction.

3. RELATED WORK

Dictionary-based MRF approaches. The original MRF reconstruction algorithm [1] is based on dictionary matching, as presented in Algorithm 1. It finds the best matching dictionary entry for the acquired temporal signature according to their inner product and then searches the lookup-table to obtain corresponding tissue parameters. Note that, $F_u^H\{\cdot\}$ denotes the inverse Fourier transform of zero-filled k-space samples, i.e. filling zeros at unknown frequencies.

Exploiting the nature of signals, by using appropriate prior knowledge, can often contribute to improved signal processing performance. Therefore, later works [3, 4] suggest to incorporate sparsity in MRF reconstruction to further improve performance, inspired by successful applications of sparsity in MRI reconstruction [7–9]. Davies et al. [3] proposed BLOch response recovery via Iterative Projection (BLIP) algorithm to exploit sparsity in the dictionary domain. BLIP consists of iterating between two main steps: (a) a gradient step which enforces consistency with the measurements, based on the Projected Landweber Algorithm (PLA) generalized from the iterative hard thresholding method; (b) a projection which matches each row of \mathbf{X} to a single dictionary atom. Instead of exploiting sparsity in the dictionary domain, Wang et al. [4] suggest to leverage sparsity in the wavelet domain of each imaging frame, $\mathbf{X}_{:,i}$. They also suggested replacing the Euclidean norm with the Mahalanobis distance for dictionary matching. Considering that adjacent MR image frames along the temporal dimension should exhibit high resemblance, recent work [5,6] proposed a magnetic resonance Fingerprint with LOW-Rank prior for reconstructing the image stack and quantitative parameters, referred to as FLOR, which achieved state-of-the-art performance. The algorithm is described in Algorithm 2.

Learning-based MRF approaches. The above approaches all use dictionary matching to perform mapping from temporal signatures to tissue parameters. Therefore, these methods suffer from drawbacks such as discretization error, slow inference speed and memory-consuming storage. In order to alleviate these issues, recent works [10, 11] propose to exploit neural networks to replace dictionaries and lookup-tables used in conventional MRF reconstruction approaches. Cohen et al. suggest a fully-connected feed-forward neural network (FNN) [10]. Since the input layer of the FNN network is fully connected with the input temporal signature, the number of neurons in the input layer corresponds to the length of the input temporal signature. This makes the network structure less flexible, as a FNN network trained on temporal signatures with a certain length is not applicable to temporal signatures

Algorithm 1 Original MRF method [1]**Input:**A set of subsampled k-space images: \mathbf{Y} A pre-simulated dictionary: \mathbf{D} An appropriate lookup-table: **LUT****Output:**Magnetic parameter maps: \hat{T}_1, \hat{T}_2 **Step 1. Restore signatures:**

$$\hat{\mathbf{X}}_{:,i} = F_u^H \{\mathbf{Y}_{:,i}\}, \forall i$$

Step 2. Restore parameters for every j via dictionary matching:

$$\hat{k}_j = \arg \max_k \frac{\mathbf{Re} \langle \mathbf{D}_{k,:}, \hat{\mathbf{X}}_{j,:} \rangle}{\|\mathbf{D}_{k,:}\|_2^2}$$

where, symbol $\mathbf{Re} \langle \mathbf{a}, \mathbf{b} \rangle$ represents the real part of the inner product of two vectors \mathbf{a} and \mathbf{b} .

$$\hat{T}_1^j, \hat{T}_2^j = \mathbf{LUT}(\hat{k}_j)$$

with a different length. In addition, the fully-connected structure results in rapid increase in the number of parameters along with the growth of depth, making the network more susceptible to overfitting. Hoppe et al. [11] propose a 3-layer convolutional neural network (CNN) for the parameter restoration purpose. Both [10] and [11] focus exclusively on learning the signature-to-parameter mapping from a pair of dictionary and lookup-table simulated using the Bloch equations. During the validation, they assume that clean temporal signatures are already available to be input into the trained networks. However, since temporal signatures obtained from k-space subsampled MRF data are always contaminated by aliasing and noise, their approaches, when applied directly in such k-space subsampling situations, can suffer from heavy artifacts introduced during the signature restoration phase, leading to poor performance.

Different from [10] and [11], we design a deep residual CNN for capturing signature-to-parameter mapping. In addition, it is organically combined with low-rank based de-aliasing techniques for signature restoration. In this way, our approach can bypass many of the issues associated with other approaches: (1) First, our approach can ingest temporal signatures with different lengths without the need to change the structure of the network. This is due to the fact that we rely on residual CNNs rather than FNNs; (2) Second, our approach involving the hybrid of a neural network with a low-rank based de-aliasing approach can also deal with possible correlations both over time and space, thus is able to handle k-space subsampling situations; (3) Third, by exploiting residual network structure, our MRF-ResNet can be successfully extended to deeper level and thus obtain better capacity to learn complex signature-to-parameter mapping functions.

Algorithm 2 FLOR [6]**Input:**A set of subsampled k-space images: \mathbf{Y} A pre-simulated dictionary: \mathbf{D} An appropriate lookup-table: **LUT**Parameters μ for gradient step and λ for regularization**Output:**Magnetic parameter maps: \hat{T}_1, \hat{T}_2 **Initialization:** $\hat{\mathbf{X}}^0 = 0, \mathbf{P} = \mathbf{D}^\dagger \mathbf{D}$, where \mathbf{D}^\dagger is the pseudo-inverse of \mathbf{D} .**Step 1. Restore signatures via iterating until convergence:**

- Gradient step for every i :

$$\hat{\mathbf{Z}}_{:,i}^{t+1} = \hat{\mathbf{X}}_{:,i}^t - \mu F_u^H \{F_u \{\hat{\mathbf{X}}_{:,i}^t\} - \mathbf{Y}_{:,i}\} \quad (6)$$

where, the superscript t represents the index of iterations.

- Project onto the dictionary subspace:

$$[\mathbf{U}, \mathbf{S}, \mathbf{V}] = \text{svd}(\hat{\mathbf{Z}}^{t+1} \mathbf{P}) \quad (7)$$

where, svd denotes the singular-value decomposition operation. \mathbf{U} and \mathbf{V} are unitary matrices that contain left-singular vectors and right-singular vectors, respectively. $\mathbf{S} = \text{diag}(\{\sigma_j\})$ is a rectangular diagonal matrix with singular values $\{\sigma_j\}$ on the diagonal.

- Soft-threshold the non-zero singular values $\{\sigma_j\}$ with parameter $\lambda\mu$ and reconstruct signatures $\hat{\mathbf{X}}^{t+1}$:

$$\begin{aligned} \sigma'_j &= \max\{\sigma_j - \lambda\mu, 0\} \\ \hat{\mathbf{X}}^{t+1} &= \mathbf{U} \mathbf{S}' \mathbf{V}^H \end{aligned} \quad (8)$$

where, $\mathbf{S}' = \text{diag}(\{\sigma'_j\})$.

Step 2. Restore parameters for every j via dictionary matching:

$$\hat{k}_j = \arg \max_k \frac{\mathbf{Re} \langle \mathbf{D}_{k,:}, \hat{\mathbf{X}}_{j,:} \rangle}{\|\mathbf{D}_{k,:}\|_2^2}$$

$$\hat{T}_1^j, \hat{T}_2^j = \mathbf{LUT}(\hat{k}_j)$$

4. PROPOSED MRF APPROACH

The proposed hybrid deep magnetic resonance fingerprinting (HYDRA) approach, summarized in Algorithm 3, consists of two stages: signature restoration and parameter restoration, (see also (5)). As illustrated in Fig. 3, a low-rank based de-aliasing method is used to restore signatures, and then a 1D residual convolutional neural network is used to map each restored signature to corresponding tissue parameters.

In particular, given Θ^{TRE} and k-space samples \mathbf{Y} , in our proposed approach, the function $\mathbf{X} = h(\mathbf{Y})$ in (5) represents a signature restoration operation using low-rank based de-aliasing techniques without requiring for a dictionary, and the function $\Theta_{j,:}^{T12} = g(\mathbf{X}_{j,:} | \Theta^{TRE})$ in (5) represents a parameter restoration operation that exploits a trained neural network to map each restored signature $\mathbf{X}_{j,:}$ to corresponding tissue parameters $\Theta_{j,:}^{T12}$ directly. In the subsequent sec-

Algorithm 3 Proposed MRF reconstruction approach

Input:A set of subsampled k-space images: \mathbf{Y} The trained MRF-ResNet: g Parameters μ for gradient step and λ for regularization**Output:** Magnetic parameter maps \hat{T}_1, \hat{T}_2 **Initialization:** $\hat{\mathbf{X}}^0 = 0$ **Step 1. Restore signatures via iterating until convergence:**

- Gradient step for every i , the same as (6).
- Perform SVD:

$$[\mathbf{U}, \mathbf{S}, \mathbf{V}] = \text{svd}(\hat{\mathbf{Z}}^{t+1})$$

- Soft-threshold the non-zero singular values $\{\sigma_j\}$ of \mathbf{S} with parameter $\lambda\mu$ and reconstruct signatures $\hat{\mathbf{X}}^{t+1}$, the same as (8).

Step 2. Restore parameters for every j via the trained MRF-ResNet:

$$\hat{T}_1^j, \hat{T}_2^j = g(\hat{\mathbf{X}}_{j,:})$$

tions, we will provide a detailed introduction to our approach, including the low-rank based signature restoration technique and the learning-based parameter restoration technique.

4.1. Low-rank based signature restoration

Since MRF data consists of multiple frames exhibiting temporal similarity across time points, the imaging contrasts matrix \mathbf{X} is typically a low-rank matrix [6]. Therefore, $h(\cdot)$ leverages a low-rank prior for denoising and de-aliasing, formulated as

$$h(\mathbf{Y}) = \arg \min_{\mathbf{X}} \frac{1}{2} \sum_i \|\mathbf{Y}_{:,i} - F_u\{\mathbf{X}_{:,i}\}\|_2^2 \quad \text{s.t.} \quad \text{rank}(\mathbf{X}) < r \quad (9)$$

where the parameter r is the rank of the matrix, a fixed pre-chosen parameter. Since typically r is not known in advance, we consider a relaxed regularized version:

$$h(\mathbf{Y}) = \arg \min_{\mathbf{X}} \frac{1}{2} \sum_i \|\mathbf{Y}_{:,i} - F_u\{\mathbf{X}_{:,i}\}\|_2^2 + \lambda \|\mathbf{X}\|_* \quad (10)$$

where $\|\mathbf{X}\|_*$ denotes the nuclear norm of \mathbf{X} , defined as the sum of the singular values of \mathbf{X} [21], and λ is the Lagrangian multiplier manually selected for balancing between data fidelity and low-rank. Problem (10) can be solved using the incremental subgradient proximal method [22], similar as in FLOR [6]. However, the difference from FLOR [6] is the fact that we have removed the operation of projecting the temporal signal onto a dictionary, thus, our signature restoration method eliminates the requirement for a simulated dictionary. The procedure for solving (5) is shown in Algorithm 3.

4.2. Learning-based parameter restoration

Once the imaging contrasts matrix \mathbf{X} is recovered from the k-space samples \mathbf{Y} , each temporal signature in \mathbf{X} is input into

the designed MRF-ResNet which is able to use learnt mapping functions to perform parameter restoration, formulated as:

$$\Theta_{j,:}^{T12} = g(\mathbf{X}_{j,:} | \Theta^{TRE}), \quad j \in [1, N] \quad (11)$$

where $g(\cdot)$ denotes the trained MRF-ResNet, Θ^{TRE} denotes the fixed RF sequence parameters. We next describe the MRF-ResNet structure, training and testing procedures.

Network structure.

The proposed MRF-ResNet has a 1D residual CNN architecture with short-cuts for residual learning. As illustrated in Fig. 3, it starts with two 1D convolutional layers before connecting with 4 residual blocks, and finally ends with a global-average-pooling layer followed by a fully-connected layer. Each residual block contains a max-pooling layer with stride 2, two convolution layers and a shortcut that enforces the network to learn the residual content. The filter size is set to be equal to 7 throughout convolutional layers. The number of channels, a.k.a feature maps, in the first two convolutional layers is set to 32 and then is doubled in subsequent four residual blocks until 512 in the final block. The size of feature maps in the next block halves in contrast with the previous one due to max-pooling operation. In this way, we gradually reduce temporal resolution while extract more features to increase content information. The global-average-pooling layer is used to average each feature map in order to integrate information in each channel for improved robustness to corrupted input data. This global-average-pooling layer also reduces the number of parameters significantly, thus lessening the computation cost as well as preventing over-fitting. The last fully-connected layer outputs estimated parameters, such as T1 and T2 relaxation times. The designed network contains around 5 million parameters and 15 layers in total, including 14 convolutional layers and 1 dense layer. It is trivial to adjust the number of outputs to adapt to more parameters, such as proton density. The weights are initialized using He-normal-distribution [23]. The max-norm kernel constraint [24] is exploited to regularize the weight matrix directly in order to prevent over-fitting. The MRF-ResNet can also be adapted for various MRF sequences, such as the original MRF sequence – inversion-recovery balanced steady state free-precession (IR-bSSFP) sequence, that depends also on the intrinsic df parameter. Also note that, in contrast with dictionary-matching-based approaches that output discrete parameter values [1–6], the MRF-ResNet outputs continuous values for each parameter since it captures the mapping functions. See also discussion in Section 5.2.

Our MRF-ResNet design is motivated and inspired by recent successful applications of convolutional neural networks and variants. Convolutional neural networks have been proved to be a powerful model to capture useful features from signals and images. By introducing convolution, local receptive field and weight sharing design, a CNN is capable of taking advantage of local spatial coherence and translation

invariance characteristics in the input signal, thus become especially well suited to extract relevant information at a low computational cost [14–19]. On the other hand, the residual network architecture [15, 16] provides an effective way to design and train a deeper model, since it alleviates the gradient vanishing or exploding problems by propagating gradients throughout the model via short-cuts, a.k.a skip connections.

Network training.

The MRF-ResNet is trained on a pair of synthesized dictionary \mathbf{D} and lookup-table \mathbf{LUT} to learn the signature-to-parameter mappings $\mathbf{LUT}_{k,:} = g(\mathbf{D}_{k,:} | \Theta^{TRE}), \forall k$.

The training dataset is synthesized as follows. First, we determine the range of tissue parameters. For example, one may set T1 relaxation times to cover a range of [1, 5000] ms and T2 relaxation times to cover a range of [1, 2000] ms with an increment of 10 ms for both. Thus, the T1 and T2 values constitute a grid with dimension 500×200 , in which each point represents a specific combination of T1 and T2 values, and hence characterize a specific tissue. Note, those points corresponding to $T1 < T2$ have been excluded as such combinations have no physical meaning. All the valid points are stacked together to generate a lookup-table. For instance, the above setting for T1 and T2 leads to a lookup-table of dimension 80100×2 . The RF pulse sequences used in our work are fast imaging with steady state precession (FISP) pulse sequences, similar to [2, 6]. Given the lookup-table and RF pulse sequences, dictionary entries can be synthesized by solving the Bloch equations using the extended phase graph formalism [25, 26].

When the training dataset is ready, the dictionary entries are used as input signals and corresponding lookup-table entries serve as the groundtruth. All the dictionary entries are input into the MRF-ResNet batch by batch and the MRF-ResNet outputs estimated parameters. The root mean square errors (RMSE) of the outputs are calculated with respect to corresponding groundtruth. The resulting RMSE loss is then backpropagated from the output layer to the first layer to update the MRF-ResNet weights and bias by using Adam [27] as the optimization algorithm. More training details are provided in the subsequent experiment section. Once the MRF-ResNet is trained well, given an inquiry temporal signature $\mathbf{X}_{j,:}$, it is able to map the input time sequence directly to corresponding tissue parameters, as formulated in (11), implying that there is no need to store the dictionary and lookup-table any more after training. Instead, we only need to store the trained MRF-ResNet, a more compact model consuming less memory than the dictionary and lookup-table.

We need to emphasize that even though the MRF-ResNet is trained on a grid of tissue values, it is expected to capture the mapping function from signatures to tissue parameters. Thus the trained MRF-ResNet is capable of outputting tissue values not existing in the grid of training values. For example, the tissue values (T1,T2)=(3333, 1333) are not in the training dataset, but the MRF-ResNet is still able to map a correspond-

Table 1. Brief description of experiment types and settings.

Experiment	Settings
Training	Input: \mathbf{D} , size $K \times L = 80100 \times 200$; Groundtruth: \mathbf{LUT} , size 80100×2 ; k-space subsampling factor β : not available;
Testing on synthetic data	Input: \mathbf{X} , size $N \times L = 80000 \times 200$; Groundtruth: Θ^{T12} , size 80000×2 ; k-space subsampling factor β : not available;
Testing on phantom data	Input: \mathbf{Y} , size $Q \times L = 16384\alpha \times 200$; Reference: Θ^{T12} , size $N \times 2 = 16384 \times 2$; k-space subsampling factor β : 100%, 70%, 15% ;

ing temporal signature to these values. Detailed results can be found in Fig. 7 and Table 2. This feature is significantly favorable, as it implies that well designed and trained networks have an ability to overcome discretization issues.

The overall procedures for solving (10) and (11) are shown in Algorithm 3. The differences from FLOR [6] include that we exploit a network for signature-to-parameter mapping, and that we do not use a dictionary either for signature restoration or for parameter restoration.

5. EXPERIMENTS

In this section, we conduct a series of experiments to evaluate our approach, comparing it with other state-of-the-art MRF methods, including [1, 3, 6, 10, 11].

The experiments are categorized into 3 types: training, testing on synthetic data, and testing on phantom data, as described in Table 1. In brief, for the network training, synthesized temporal signatures, i.e. simulated dictionary entries of \mathbf{D} shown as Fig.4, are used as input signals and corresponding parameter values in the lookup-table \mathbf{LUT} serve as the groundtruth. The MRF-ResNet is trained to capture the signature-to-parameter mappings. For the testing on synthetic data, synthesized temporal signatures in \mathbf{X} are used as input signals and corresponding parameter values in Θ^{T12} serve as the groundtruth. The aim is to test the parameter restoration performance only. For the testing on phantom data, the k-space measurements \mathbf{Y} , derived from the Fourier transform of \mathbf{X} are used as input and corresponding parameter values in Θ^{T12} serve as reference. When there is no k-space subsampling, the aim is to test the parameter restoration performance only. When there exists k-space subsampling, the aim is to test the overall performance, including both signature restoration and parameter restoration. More detailed descriptions are provided in each subsection.

5.1. Training

As mentioned in Section 4.2, the designed MRF-ResNet is trained on a pair of synthesized dictionary \mathbf{D} and lookup-table \mathbf{LUT} , simulated using Bloch equations and FISP pulse sequences [2, 6].

The FISP pulse sequence was designed with parameters $\Theta_{:,i}^{TRE} = [TR^i, TE^i, FA^i]^T, i \in [1, L]$, where the echo time

TE^i is constant of 2ms, the repetition time TR^i has a random value in the range of 11.5 - 14.5 ms, all the flip angles $FA^i, i \in [1, L]$ constitute a sinusoidal variation in the range of 0 - 70 degrees, and the number of time points (equivalent to the number of frames) L is set to 200. For the range of tissue parameters, T1 relaxation times are set to cover a range of [1, 5000] ms and T2 relaxation times to cover a range of [1, 2000] ms with an increment of 10 ms for both. Such parameter ranges cover the relaxation time values that can be commonly found in a brain scan [28]. All the valid combinations of T1 and T2 values are stacked together, generating a lookup-table **LUT** of dimension 80100×2 with $K = 80100$. Given the lookup-table and RF pulse sequences, dictionary entries are synthesized by solving the Bloch equations using the extended phase graph formalism, leading to a dictionary of dimension $K \times L = 80100 \times 200$.

When the training dataset is ready, the dictionary entries are used as input signals and corresponding lookup-table entries serve as the groundtruth to train the MRF-ResNet, as mentioned in Section 4.2. The model was trained for 50 epochs. It takes around 30 seconds for running one epoch on average, thus around 25 minutes for completing 50 epochs, on a NVIDIA GeForce GTX 1080 Ti GPU. In each training epoch, 20% of the training samples are separated aside for validation dataset. The learning rate decays from 1e-2 to 1e-6 every 10 epochs. Each batch was experimentally set to contain 256 time-sequences in order to balance the convergence rate and weights updating rate well. For comparison purposes, we also implemented Hoppe et al.'s CNN referring to [11], and Cohen et al.'s FNN referring to [10] with the same structure and parameters as specified in their papers. Then we use the same GPU and training dataset to train their networks with specified learning rate and number of epochs until convergence.

5.2. Testing on synthetic dataset

In this subsection, we evaluate the performance of our MRF-ResNet on a synthetic testing dataset. The procedures of constructing a synthetic testing dataset is similar to the construction of the training dataset. 500 different T1 values are randomly selected from 1 - 5000 ms, while 200 different T2 values are randomly selected from 1 - 2000 ms, using random permutation based on uniformly distributed pseudorandom numbers. All the valid combinations from the selected T1 and T2 values are stacked together, generating a parameter matrix Θ^{T12} of dimension 80000×2 with $N = 80000$. The RF pulse sequences are the same as in the training stage. Given the parameter matrix and RF pulse sequences, input signal signatures are synthesized by solving the Bloch equations using the extended phase graph formalism, leading to a signature matrix \mathbf{X} of dimension $N \times L = 80000 \times 200$, with each row representing a temporal signature corresponding to a specific combination of T1 and T2 values. The signature matrix \mathbf{X} and parameter matrix Θ^{T12} constitute the synthetic

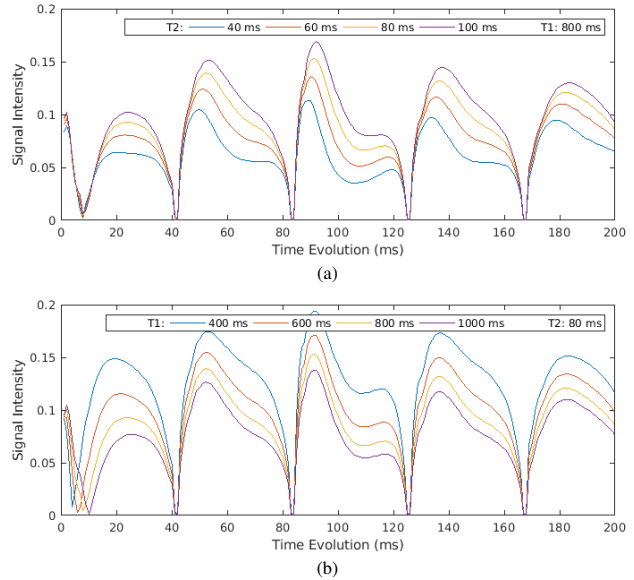


Fig. 4. Synthetic MRF temporal signatures. (a) Temporal signatures corresponding to parameter values $\{(T1, T2)\} \text{ ms} = \{(800,40);(800,60);(800,80);(800,100)\}$ ms. (2) Temporal signatures corresponding to parameter values $\{(T1, T2)\} \text{ ms} = \{(400,80);(600,80);(800,80);(1000,80)\}$ ms.

testing dataset, with \mathbf{X} as input and Θ^{T12} as the groundtruth.

We input the synthetic testing signatures \mathbf{X} into Hoppe et al.'s CNN [11], Cohen et al.'s FNN [10], and proposed MRF-ResNet and compare the outputs with groundtruth T1 and T2 values in Θ^{T12} . In comparison, the dictionary matching method used in [1–6] exploits the same dictionary \mathbf{D} and lookup-table **LUT** to find the best matching entry for each signature in \mathbf{X} and then estimate parameter values by searching the lookup-table. As shown in Table 2, Table 3, Fig. 5 and Fig. 7, the estimated parameter values using the proposed MRF-ResNet obtained outstanding agreement with the groundtruth, yielding higher PSNR, SNR and lower RMSE than the dictionary matching method [1–6], as well as competing networks [10, 11].

In particular, to illustrate in detail how well neural networks tackle the discretization issue inherent to dictionary matching, we show the testing performance on continuous-valued T1, T2 parameters which have small intervals, e.g. 0.5ms, that is 20 times smaller than the training grid intervals 10ms, between neighboring values in Table 3. Since these values and their corresponding MRF signatures do not exist in the training dictionary and lookup-table², it is noticed that the dictionary matching methods report a T1 and T2 value – the closest discretized value present in the dictionary – that can be quite distinct from the groundtruth. In contrast, the

² As mentioned in the experiment setting in section 5.1, in the training dataset, T1 relaxation times are set to cover a range of [1, 5000] ms and T2 relaxation times to cover a range of [1, 2000] ms with an increment of 10 ms for both, that is, T1 values = {1, 11, 21, ..., 4991}, and T2 values = {1, 11, 21, ..., 1991}.

Table 2. Testing on synthetic dataset. Comparing parameter restoration performance, in terms of PSNR, SNR, RMSE and correlation coefficient.

	Dict. Match. T1 / T2	CNN [11] T1 / T2	FNN [10] T1 / T2	Proposed T1 / T2
PSNR (dB)	59.15 / 52.31	62.96 / 49.64	58.97 / 54.96	79.30 / 72.99
SNR (dB)	55.23 / 47.15	59.05 / 44.49	55.06 / 49.81	75.38 / 67.83
RMSE (ms)	5.515 / 4.847	3.554 / 6.591	5.63 / 3.57	0.542 / 0.448
CorrCoef	0.99998977 / / 0.99996484	0.99999575 / / 0.99993511	0.99998942 / / 0.999981	0.99999990 / / 0.99999970
time cost (s)	464.10	2.87	1.58	8.2

Table 3. Testing on synthetic dataset involving some de-tailed T1 / T2 examples that are not on the training grid and their intervals are much smaller than the training grid intervals. D.M. denotes the dictionary matching. T1 and T2 errors are defined as the difference between estimated values and groundtruth values.

Truth	T1 Estimation				T1 Errors			
	D.M.	[11]	[10]	Ours	D.M.	[11]	[10]	Ours
1005.0	1001.0	1002.9	1009.3	1004.8	-4.0	-2.1	4.3	-0.2
1005.5	1001.0	1003.3	1010.0	1005.3	-4.5	-2.3	4.5	-0.2
1006.0	1011.0	1003.6	1010.6	1005.8	5.0	-2.4	4.6	-0.2
1006.5	1011.0	1004.1	1011.2	1006.3	4.5	-2.5	4.7	-0.2
1007.0	1011.0	1004.5	1011.8	1006.8	4.0	-2.5	4.8	-0.3
RMSE	-	-	-	-	4.4	2.3	4.6	0.2

Truth	T2 Estimation				T2 Errors			
	D.M.	[11]	[10]	Ours	D.M.	[11]	[10]	Ours
505.0	501.0	513.6	504.3	505.2	-4.0	8.6	-0.7	0.2
505.5	511.0	514.1	504.8	505.7	5.5	8.6	-0.7	0.2
506.0	501.0	514.7	505.3	506.2	-5.0	8.6	-0.7	0.2
506.5	511.0	515.2	505.9	506.8	4.5	8.7	-0.6	0.3
507.0	511.0	515.7	506.4	507.3	4.0	8.7	-0.6	0.3
RMSE	-	-	-	-	4.6	8.6	0.7	0.2

various neural network approaches can potentially learn an underlying mapping from the temporal signatures to the respective T1 and T2 values, leading to estimates that are much closer to the groundtruth. Interestingly, our approach can outperform those in [10, 11] as shown in Table 3 and Fig. 5. In this way, neural networks demonstrate much better robustness to discretization issues, leading to much better parameter restoration in comparison to dictionary based methods.

Another impressive advantage of the MRF-ResNet is the fast inference speed. It is observed that the MRF-ResNet takes only 8.2 s to complete the mapping operation for eighty thousand temporal signatures, that is, $53 \times$ faster than a dictionary based method. Furthermore, the inference speed of the MRF-ResNet is subject to the network topology. That is, once the network structure is fixed, the complexity is fixed. In contrast, the complexity of dictionary matching based methods is limited by the dictionary density. It implies that our advantage will be more prominent in comparison with competing methods using a dictionary with higher density.

5.3. Testing on phantom dataset

In this subsection, we evaluate our approach on a phantom testing dataset, in comparison with [1, 3, 6, 10, 11]. We construct the phantom testing dataset from brain scans that were acquired with GE Signa 3T HDXT scanner from a healthy

Table 4. Testing on phantom dataset without k-space subsampling. Comparing parameter restoration performance, in terms of PSNR, SNR, RMSE and correlation coefficient.

	Dict. Match. T1 / T2	CNN [11] T1 / T2	FNN [10] T1 / T2	Proposed T1 / T2
PSNR (dB)	56.64 / 52.04	54.06 / 49.88	54.53 / 54.36	56.59 / 60.01
SNR (dB)	42.20 / 27.81	39.63 / 25.66	40.09 / 30.07	42.15 / 35.76
RMSE (ms)	6.623 / 6.252	8.912 / 8.015	8.45 / 4.78	6.661 / 2.498
CorrCoef	0.99995714 / / 0.99904978	0.99992222 / / 0.99841255	0.99992949 / / 0.99945847	0.99995632 / / 0.99984786
time cost (s)	84.5635	0.69	0.41	1.6

Table 5. Testing on phantom dataset with k-space subsampling ratio 70% and 15%. Integrating signature restoration and parameter restoration for T1 / T2 mapping.

k-space subsampling factor $\beta = 70\%$			
	Ma et al. [1]	BLIP [3]	FLOR [6]
PSNR (dB)	23.69 / 38.17	45.67 / 47.84	50.11 / 50.85
SNR (dB)	8.73 / 13.84	31.28 / 23.49	35.67 / 26.48
RMSE (ms)	294.32 / 30.87	23.42 / 10.14	14.01 / 7.17
time cost (s)	72.88	75.7	85.35
k-space subsampling factor $\beta = 15\%$			
	CNN [11]	FNN [10]	Proposed
PSNR (dB)	49.71 / 45.48	50.15 / 51.08	50.79 / 51.59
SNR (dB)	35.26 / 21.19	35.70 / 26.67	36.34 / 27.19
RMSE (ms)	14.71 / 13.31	13.99 / 6.98	12.99 / 6.57
time cost (s)	23.72	23.53	24.85
k-space subsampling factor $\beta = 15\%$			
	Ma et al. [1]	BLIP [3]	FLOR [6]
PSNR (dB)	27.94 / 32.84	35.45 / 39.25	44.95 / 46.11
SNR (dB)	13.50 / 8.61	20.99 / 14.58	30.51 / 21.89
RMSE (ms)	180.3 / 57.03	76.01 / 27.25	25.46 / 12.37
time cost (s)	106	112.8	121.7
	CNN [11]	FNN [10]	Proposed
PSNR (dB)	43.74 / 35.98	45.03 / 45.90	45.23 / 44.44
SNR (dB)	29.23 / 12.26	30.58 / 21.32	30.76 / 19.78
RMSE (ms)	29.27 / 39.73	25.21 / 12.68	24.65 / 15.00
time cost (s)	24.54	24.36	25.67

subject.³ Since there are no groundtruth parameter values, we need to obtain gold standard data for reference. To generate gold standard data for the T1 and T2 parameter maps, we acquired Fast Imaging Employing Steady-state Acquisition (FIESTA) and Spoiled Gradient Recalled Acquisition in Steady State (SPGR) images, at 4 different flip angles ($3^\circ, 5^\circ, 12^\circ$ and 20°), and then implemented well known DESPOT1 and DESPOT2 [29] algorithms, after improvements as described in [30]. The constructed gold standard T1, T2 parameter maps have a dimension of 128×128 for each map, accordingly leading to a parameter matrix Θ^{T12} of size 16384×2 by stacking vectorized T1, T2 maps together. Based on the parameter matrix Θ^{T12} and pre-defined RF pulse sequences, we generate temporal signatures using Bloch equations, the same mechanism as generating the synthetic testing dataset, leading to a signature matrix \mathbf{X} of dimension $N \times L = 16384 \times 200$. The signature matrix \mathbf{X} and parameter matrix Θ^{T12} constitute the phantom testing dataset, with \mathbf{X} as input and Θ^{T12} as the gold standard reference.

³The experiment procedures involving human subjects described in this paper were approved by the Institutional Review Board of Tel-Aviv Sourasky Medical Center, Israel.

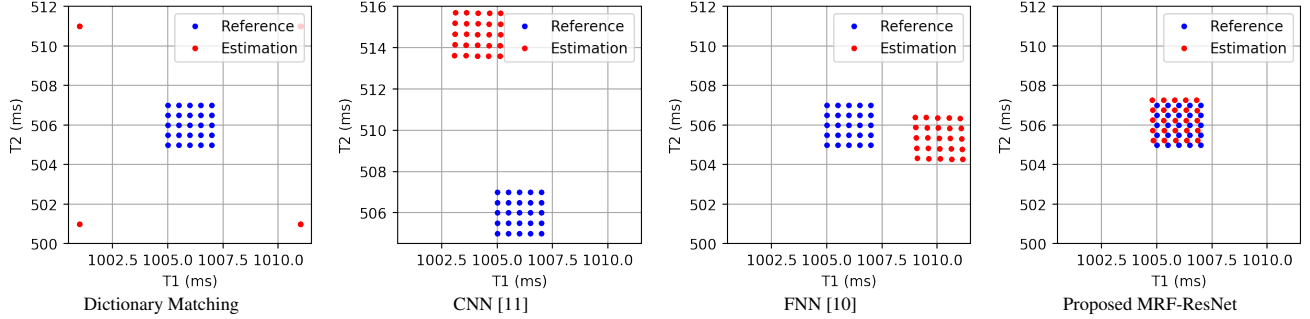


Fig. 5. Testing on synthetic dataset involving some detailed T1 / T2 examples that are not on the training grid and their intervals are much smaller than the training grid intervals. It is noticed that dictionary matching finds best adjacent values from the dictionary, i.e. 1001, 1011 for T1, and 501, 511 for T2. In contrast, owing to the captured mapping functions, neural networks output well-estimated continuous values. The proposed MRF-ResNet leads to least deviations and bias.

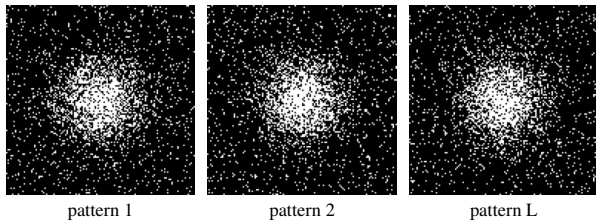


Fig. 6. A series of k-space subsampling patterns.

Note that, since the gold standard T1, T2 maps exhibit spatial structures in the image domain, the resulting signature matrix \mathbf{X} can be regarded as a stack of $L = 200$ vectorized image frames, where each frame exhibits specific spatial structures. Therefore, it makes sense to perform Fourier transform and k-space subsampling for each column of \mathbf{X} to get k-space measurements \mathbf{Y} . This is the key difference of the phantom dataset from the synthetic dataset.

We first explore the situation without k-space subsampling in order to evaluate the parameter restoration performance of the proposed MRF-ResNet. Then, we also explore the situations with k-space subsampling in order to evaluate both the signature restoration and the parameter restoration performance of the proposed approach HYDRA.

Without k-space subsampling.

In this situation, the fully-sampled k-space measurements \mathbf{Y} , derived from the Fourier transform of \mathbf{X} , are used as the input to obtain the estimated Θ^{T12} . This is equivalent to input \mathbf{X} into the MRF-ResNet, or perform dictionary matching based on \mathbf{X} directly, since the inverse Fourier transform of the fully-sampled measurements \mathbf{Y} is exactly the same as \mathbf{X} . The aim is to test the parameter restoration performance only. In the experiment, corresponding parameter values in Θ^{T12} serve as the gold standard reference. For comparison, dictionary matching method used in [1–6] exploits the same dictionary \mathbf{D} and lookup-table \mathbf{LUT} as in our training stage to find the best matching entry and estimate parameter values for each signature in \mathbf{X} .

The visual and quantitative results are shown in Fig. 8, Fig. 9 and Table 4. It is noticed that our approach outperforms

the dictionary matching method used in [1–6], yielding better both visual and quantitative performance, e.g., 7.9dB SNR gains for T2 mapping. The RMSE of T2 mapping is also reduced to 2.498 from 6.252, accordingly. This is owing to the advantage that the trained neural MRF-ResNet is a powerful function approximator. It outputs well-estimated parameter values based on learnt mapping functions, even though these values do not exist in the training dictionary and lookup-table. In addition, similar trend is observed that our deep residual network outperforms competing networks such as Hoppe et al.’s CNN [11] and Cohen et al.’s FNN [10]. In contrast, the dictionary matching method only matches signatures to discrete parameters existing in the training grid. In addition, the MRF-ResNet takes only 1.6 s to accomplish the mapping for 16384 signatures, $56\times$ faster than the dictionary matching operation used in [1–6].

With k-space subsampling.

In k-space subsampling situations, the developed low-rank based de-aliasing method is applied to restore the signature matrix \mathbf{X} from the measurements matrix \mathbf{Y} . Then, the reconstructed \mathbf{X} is input into the MRF-ResNet for parameter mapping to obtain the corresponding tissue parameter values. In the experiments, the sub-sampling factor β is set to be 70% and 15%. For $\beta = 15\%$, 15% k-space data is acquired by a series of 2D random Gaussian sampling patterns, shown in Fig. 6, leading to a k-space measurement matrix \mathbf{Y} of size $Q \times L = 2458 \times 200$. Similarly, $\beta = 70\%$ gives rise to a k-space measurement matrix \mathbf{Y} of size $Q \times L = 11469 \times 200$. The Since a larger λ enforces lower rank for the restored signature matrix \mathbf{X} to strengthen de-aliasing effect, while a smaller λ encourages \mathbf{X} to have an subsampled Fourier transform that approximates to the k-space measurements matrix \mathbf{Y} better, we tried a range of values from 1 to 20 for λ and experimentally select the best one $\lambda = 5$. Considering that the low-rank based signature restoration involves gradient descent steps, a larger step size μ accelerates gradient descent speed, but tend to result in oscillation or even divergence, while a smaller μ leads to a slow convergence speed. We

experimentally find that $\mu = 1$ gives a good balance. The same k-space measurements \mathbf{Y} is also used by dictionary-matching-based methods [1, 3, 6] for comparison, and the same signature restoration approach is also used to convert \mathbf{Y} onto \mathbf{X} for deep-learning-based methods [10, 11]. The aim is to evaluate the overall performance on both signature restoration and parameter restoration.

The visual and quantitative performance is shown in Fig. 10, Fig. 11 and Table 5. It is noticed that the advantage of deep learning methods over dictionary matching methods degrades when the subsampling factor increases. This is due to the fact that the restored signatures from highly subsampled k-space data exhibit stronger deviations from the groundtruth, thus leading to poorer input for the trained networks. In spite of this, the proposed approach outperforms the dictionary matching based method [1] with significant gains, and also yields better or competitive performance as the state-of-the-art methods FLOR [6], CNN [11] and FNN [10]. In addition, our method takes around 24s for low-rank based signature restoration and around 1.7s for network-based parameter restoration. So total time cost around 25.7s, almost $4.8\times$ faster than FLOR [6]. Furthermore, the speed of our method is $60\times$ faster than FLOR [6] for parameter restoration stage.

We also note that storing the MRF-ResNet with 5 million parameters requires 20.3 megabytes while storing the simulated dictionary of size 80100×200 requires more than 100 megabytes when using double precision for both. Note that the dictionary volume will grow exponentially with the number of parameters, but the space required for storing a network is not strictly limited by the dictionary density once the topology of the network is fixed, thus significantly alleviating the storage burden inherent to the exponential growth of multi-dimensional dictionaries.

6. CONCLUSION

We proposed a hybrid deep MRF approach which combines a low-rank based signature restoration and a learning-based parameter restoration. In our approach, a low-rank based de-aliasing method is used to restore clean signatures from subsampled k-space measurements. Then, a 1D deep residual convolutional neural network is used for efficient signature-to-parameter mapping, replacing the time-consuming dictionary matching operation in conventional MRF approaches. Our approach demonstrates advantages in terms of inference speed, accuracy and storage requirements over competing MRF methods as no dictionary is needed for recovery.

7. REFERENCES

- [1] D. Ma, V. Gulani, N. Seiberlich, K. Liu, J. L. Sunshine, J. L. Duerk, and M. A. Griswold, "Magnetic resonance fingerprinting," *Nature*, vol. 495, no. 7440, p. 187, 2013.
- [2] Y. Jiang, D. Ma, N. Seiberlich, V. Gulani, and M. A. Griswold, "MR fingerprinting using fast imaging with steady state precession (fisp) with spiral readout," *Magnetic resonance in medicine*, vol. 74, no. 6, pp. 1621–1631, 2015.
- [3] M. Davies, G. Puy, P. Vandergheynst, and Y. Wiaux, "A compressed sensing framework for magnetic resonance fingerprinting," *SIAM Journal on Imaging Sciences*, vol. 7, no. 4, pp. 2623–2656, 2014.
- [4] Z. Wang, H. Li, Q. Zhang, J. Yuan, and X. Wang, "Magnetic resonance fingerprinting with compressed sensing and distance metric learning," *Neurocomputing*, vol. 174, pp. 560–570, 2016.
- [5] G. Mazor, L. Weizman, A. Tal, and Y. C. Eldar, "Low rank magnetic resonance fingerprinting," in *Engineering in Medicine and Biology Society (EMBC), 2016 IEEE 38th Annual International Conference of the*. IEEE, 2016, pp. 439–442.
- [6] G. Mazor, L. Weizman, A. Tal, and Y. C. Eldar, "Low-rank magnetic resonance fingerprinting," *Medical physics*, vol. 45, no. 9, pp. 4066–4084, 2018.
- [7] M. Lustig, D. L. Donoho, J. M. Santos, and J. M. Pauly, "Compressed sensing MRI," *IEEE signal processing magazine*, vol. 25, no. 2, pp. 72–82, 2008.
- [8] L. Weizman, Y. C. Eldar, and D. Ben Bashat, "Compressed sensing for longitudinal MRI: An adaptive-weighted approach," *Medical physics*, vol. 42, no. 9, pp. 5195–5208, 2015.
- [9] L. Weizman, Y. C. Eldar, and D. Ben Bashat, "Reference-based MRI," *Medical physics*, vol. 43, no. 10, pp. 5357–5369, 2016.
- [10] O. Cohen, B. Zhu, and M. S. Rosen, "MR fingerprinting deep reconstruction network (drone)," *Magnetic resonance in medicine*, vol. 80, no. 3, pp. 885–894, 2018.
- [11] E. Hoppe, G. Körzdörfer, T. Würfl, J. Wetzl, F. Lugauer, J. Pfeuffer, and A. Maier, "Deep learning for magnetic resonance fingerprinting: A new approach for predicting quantitative parameter values from time series," *Stud Health Technol Inform*, vol. 243, pp. 202–206, 2017.
- [12] Y. LeCun, Y. Bengio, and G. Hinton, "Deep learning," *Nature*, vol. 521, no. 7553, p. 436, 2015.
- [13] I. Goodfellow, Y. Bengio, A. Courville, and Y. Bengio, *Deep learning*. MIT press Cambridge, 2016, vol. 1.
- [14] A. Krizhevsky, I. Sutskever, and G. E. Hinton, "Imagenet classification with deep convolutional neural networks," in *Advances in neural information processing systems*, 2012, pp. 1097–1105.

- [15] K. He, X. Zhang, S. Ren, and J. Sun, "Deep residual learning for image recognition," in *Proc. IEEE Conf. Comput. Vision Pattern Recog*, 2016, pp. 770–778.
- [16] K. He, X. Zhang, S. Ren, and J. Sun, "Identity mappings in deep residual networks," in *Proc. Eur. Conf. Comput. Vision*. Springer, 2016, pp. 630–645.
- [17] C. Dong, C. C. Loy, K. He, and X. Tang, "Image super-resolution using deep convolutional networks," *IEEE Trans. Pattern Anal. Mach. Intell.*, vol. 38, no. 2, pp. 295–307, 2016.
- [18] J. Kim, J. Kwon Lee, and K. Mu Lee, "Deeply-recursive convolutional network for image super-resolution," in *Proc. IEEE Conf. Comput. Vision Pattern Recog*, 2016, pp. 1637–1645.
- [19] J. Gehring, M. Auli, D. Grangier, D. Yarats, and Y. N. Dauphin, "Convolutional sequence to sequence learning," *arXiv preprint arXiv:1705.03122*, 2017.
- [20] G. Hinton, L. Deng, D. Yu, G. E. Dahl, A.-r. Mohamed, N. Jaitly, A. Senior, V. Vanhoucke, P. Nguyen, T. N. Sainath *et al.*, "Deep neural networks for acoustic modeling in speech recognition: The shared views of four research groups," *IEEE Signal processing magazine*, vol. 29, no. 6, pp. 82–97, 2012.
- [21] J.-F. Cai, E. J. Candès, and Z. Shen, "A singular value thresholding algorithm for matrix completion," *SIAM Journal on Optimization*, vol. 20, no. 4, pp. 1956–1982, 2010.
- [22] S. Sra, S. Nowozin, and S. J. Wright, *Optimization for machine learning*. Mit Press, 2012.
- [23] K. He, X. Zhang, S. Ren, and J. Sun, "Delving deep into rectifiers: Surpassing human-level performance on imagenet classification," in *Proc. IEEE Int. Conf. Comput. Vision*, 2015, pp. 1026–1034.
- [24] N. Srivastava, G. Hinton, A. Krizhevsky, I. Sutskever, and R. Salakhutdinov, "Dropout: a simple way to prevent neural networks from overfitting," *The Journal of Machine Learning Research*, vol. 15, no. 1, pp. 1929–1958, 2014.
- [25] J. Hennig, "Echoes? how to generate, recognize, use or avoid them in mr-imaging sequences. part i: Fundamental and not so fundamental properties of spin echoes," *Concepts in Magnetic Resonance*, vol. 3, no. 3, pp. 125–143, 1991.
- [26] M. Weigel, "Extended phase graphs: dephasing, rf pulses, and echoes-pure and simple," *Journal of Magnetic Resonance Imaging*, vol. 41, no. 2, pp. 266–295, 2015.
- [27] D. P. Kingma and J. Ba, "Adam: A method for stochastic optimization," *arXiv preprint arXiv:1412.6980*, 2014.
- [28] J. Vymazal, A. Righini, R. A. Brooks, M. Canesi, C. Mariani, M. Leonardi, and G. Pezzoli, "T1 and t2 in the brain of healthy subjects, patients with parkinson disease, and patients with multiple system atrophy: relation to iron content," *Radiology*, vol. 211, no. 2, pp. 489–495, 1999.
- [29] S. C. Deoni, T. M. Peters, and B. K. Rutt, "High-resolution t1 and t2 mapping of the brain in a clinically acceptable time with despot1 and despot2," *Magnetic Resonance in Medicine: An Official Journal of the International Society for Magnetic Resonance in Medicine*, vol. 53, no. 1, pp. 237–241, 2005.
- [30] G. Liberman, Y. Louzoun, and D. Ben Bashat, "T1 mapping using variable flip angle spgr data with flip angle correction," *Journal of Magnetic Resonance Imaging*, vol. 40, no. 1, pp. 171–180, 2014.

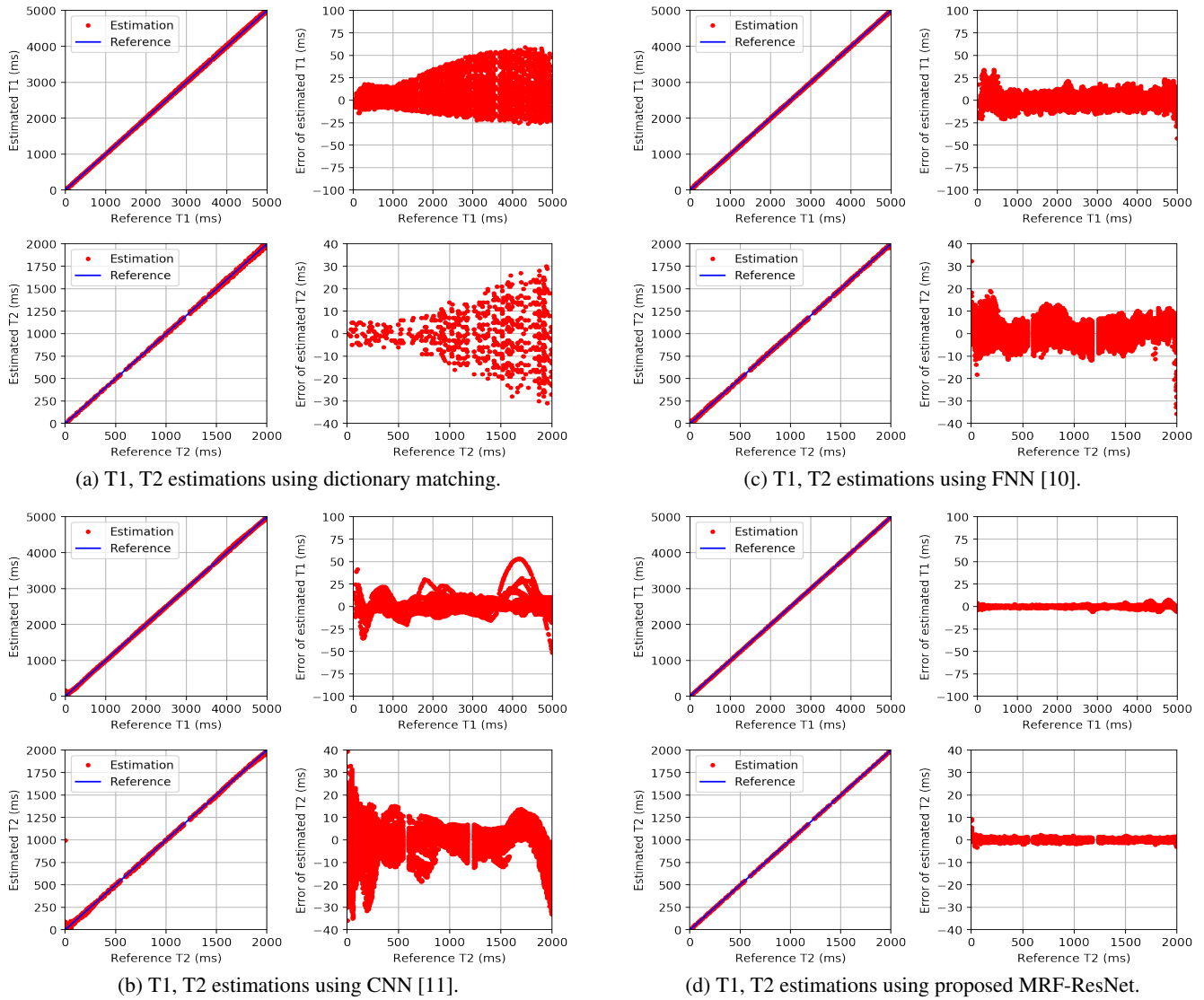


Fig. 7. Testing on the synthetic dataset for comparing parameter restoration performance. Subfig. (a) - (d) show the results using dictionary matching [1–6], FNN [10], CNN [11] and proposed MRF-ResNet. In each subfigure, the left figure compares the estimated T1 or T2 values (marked with red dot) with groundtruth values (marked with blue line), and the right figure shows the deviations of the estimation from the groundtruth. It is noticed that the parameter mapping performance using the trained MRF-ResNet is much better than competing methods, in the entire value range of T1 and T2 parameters, resulting in smaller deviations. The performance is also verified by some quantitative metrics, as shown in Table 2.

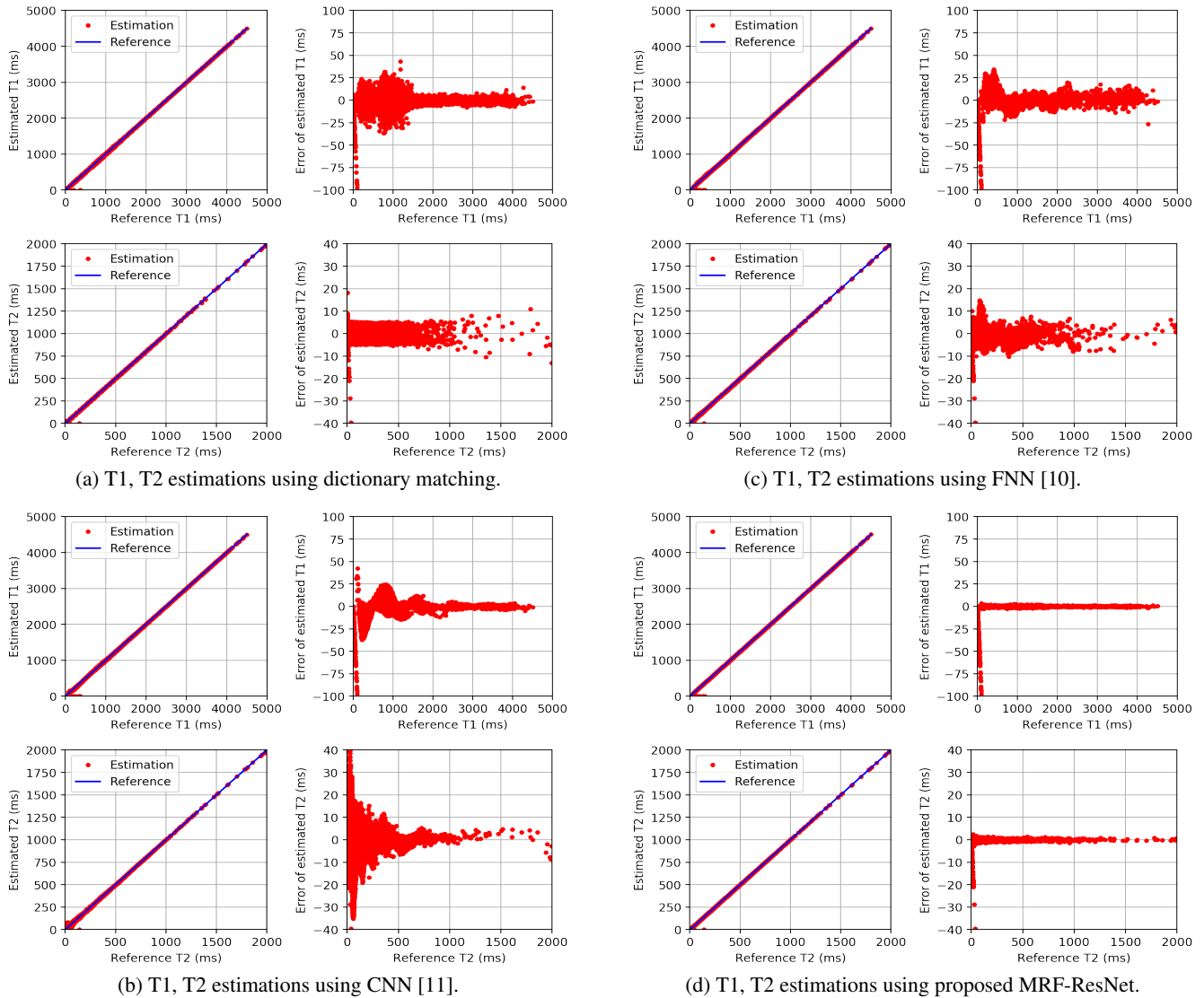


Fig. 8. Testing on the phantom dataset without k-space subsampling for comparing parameter restoration performance. Subfig. (a) - (d) show the results using dictionary matching [1–6], FNN [10], CNN [11] and proposed MRF-ResNet. In each subfigure, the left figure compares the estimated T1 or T2 values (marked with red dot) with reference values (marked with blue line), and the right figure shows the deviations of the estimation from the reference. It is also noticed that the parameter mapping performance using the trained MRF-ResNet outperforms competing methods significantly, resulting in smaller deviations. The performance is also verified by some quantitative metrics, as shown in Table 4.

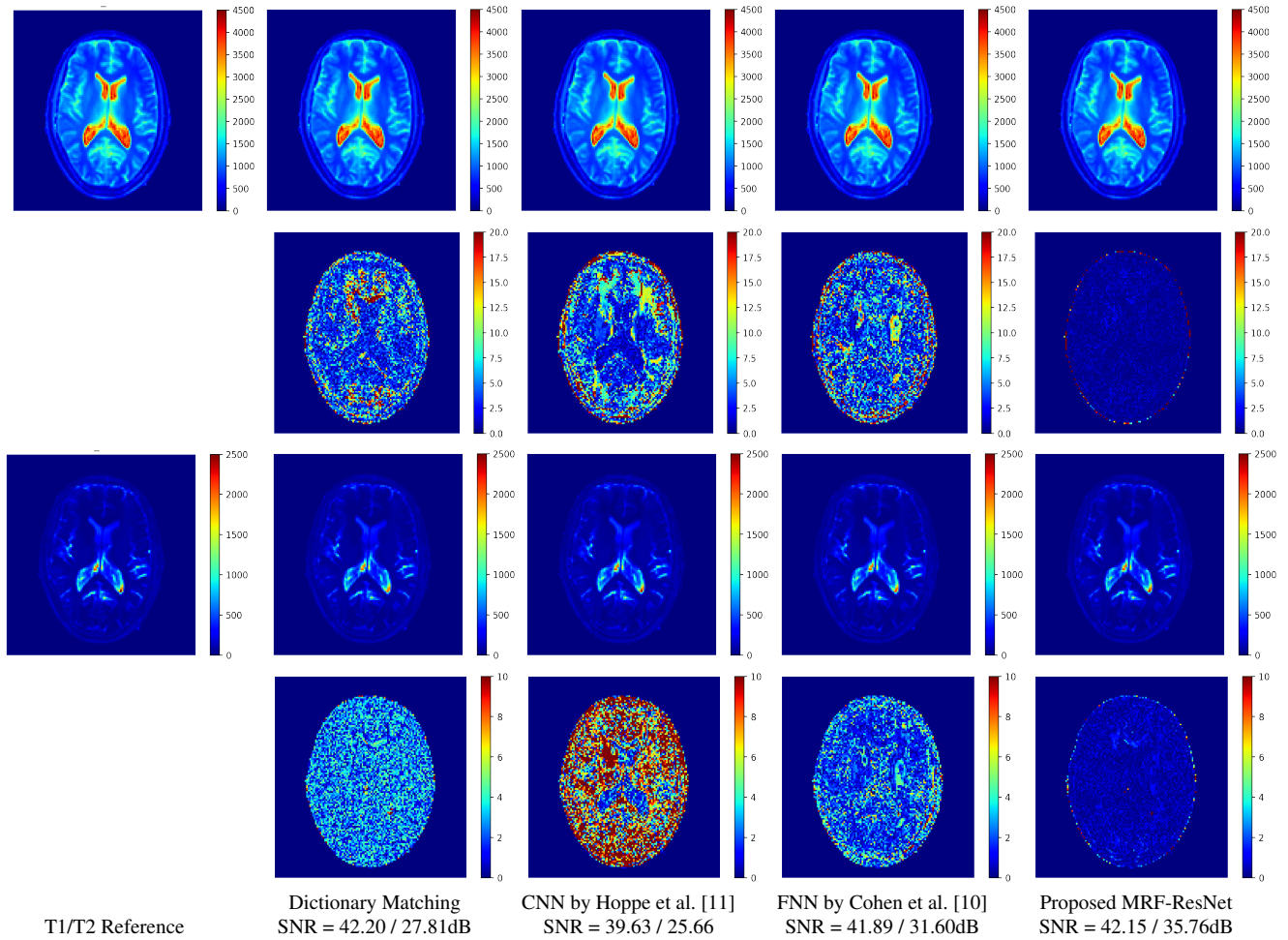
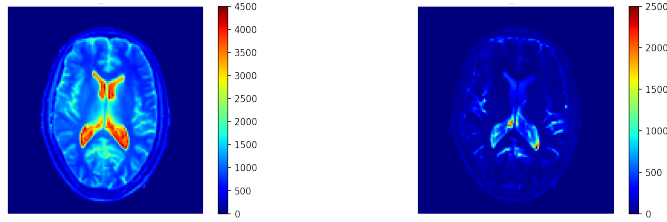
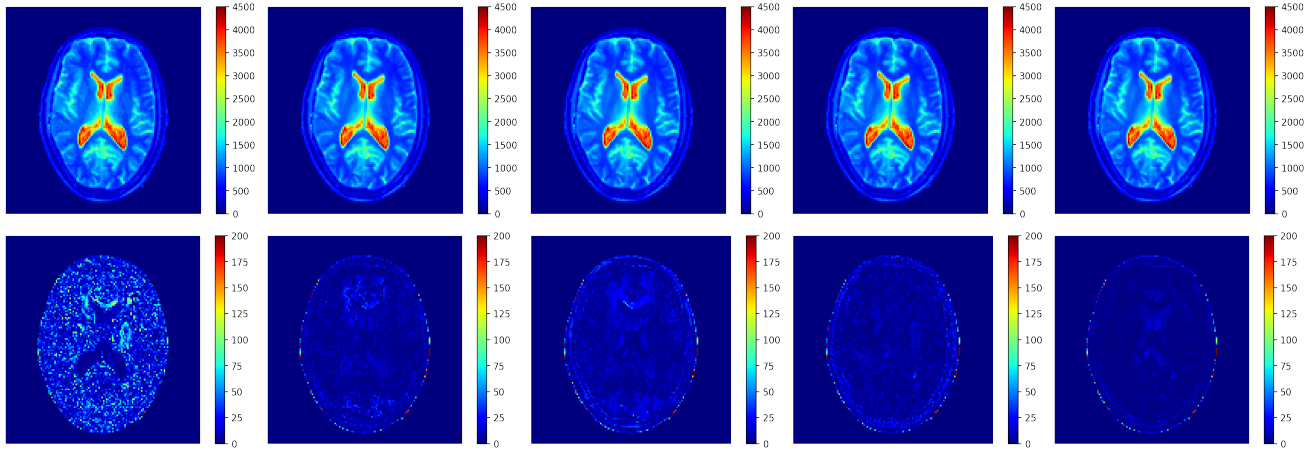


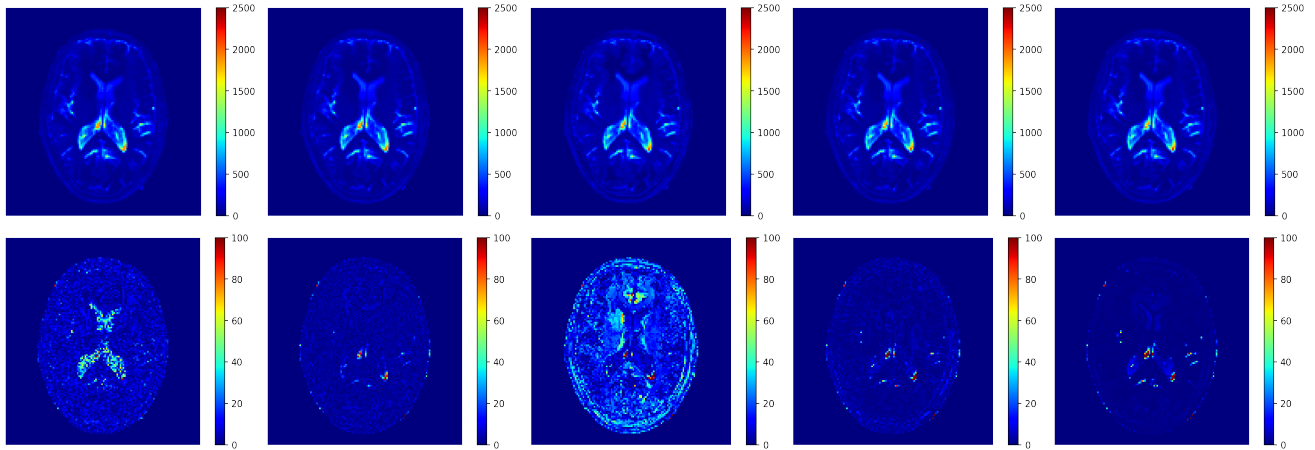
Fig. 9. Visual results of testing on phantom dataset without k-space subsampling for comparing parameter restoration performance. Top two rows correspond to T1 maps and residual errors while bottom two rows correspond to T2 maps and residual errors. It is noticed that the proposed MRF-ResNet gives competitive performance for T1 mapping and yields much better performance for T2 mapping, obtaining 7.9dB SNR higher gains than the competing dictionary-matching-based methods [1–6]. The proposed MRF-ResNet also outperforms deep-learning-based methods, such as CNN by Hoppe et al. [11] and FNN by Cohen et al. [10]. In addition, the proposed MRF-ResNet takes only 1.6 s to accomplish the mapping for a pair of T1 / T2 parameter maps of size 128 x 128, that is 56x faster than the dictionary matching method. (Zoom-in in a electric screen for better visualization)



(a) T1 reference (left) and T2 reference (right).



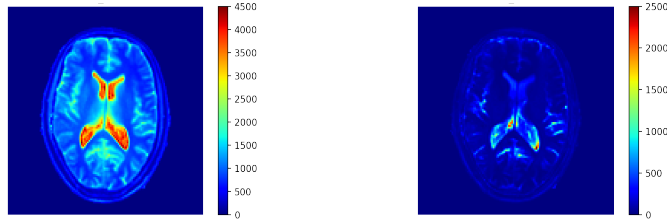
(b) T1 estimation (top row) and residual errors (bottom row).



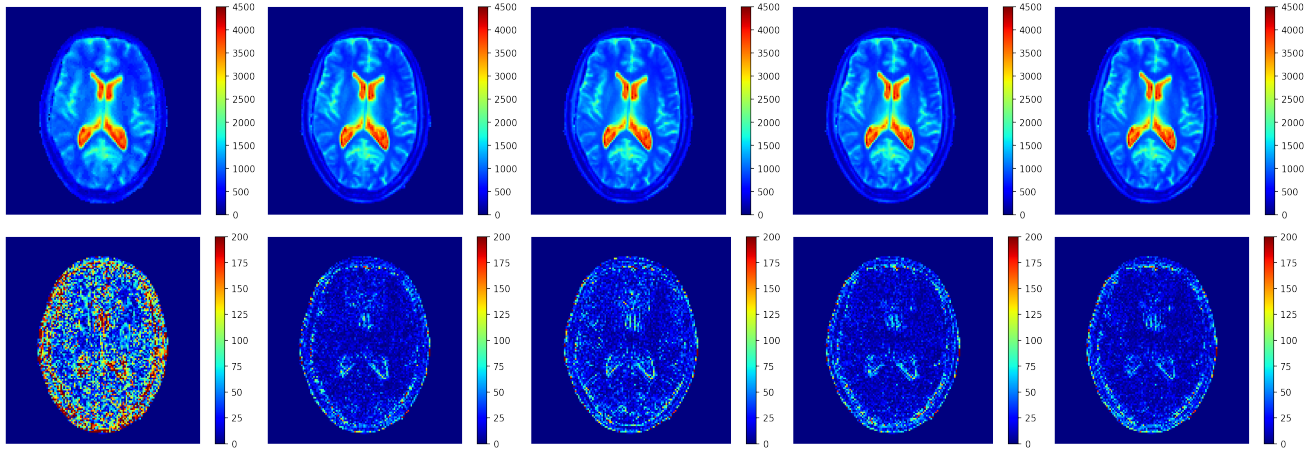
(c) T2 estimation (top row) and residual errors (bottom row).

BLIP [3]	FLOR [6]	CNN [11]	FNN [10]	proposed HYDRA
SNR = 31.28 / 23.49 dB	SNR = 35.67 / 26.48 dB	SNR = 35.26 / 21.19 dB	SNR = 35.70 / 26.67 dB	SNR = 36.34 / 27.19 dB

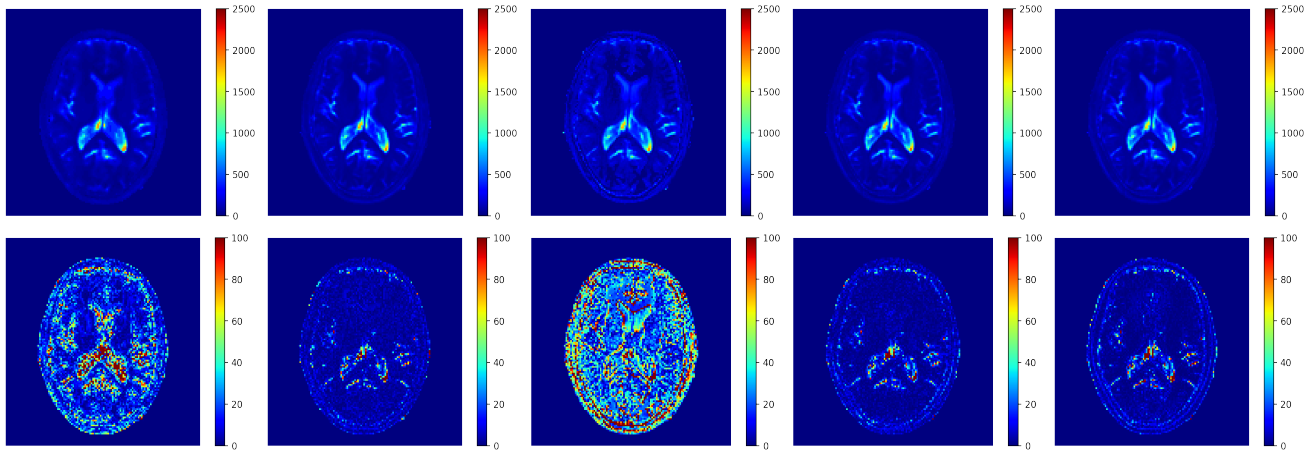
Fig. 10. Visual results of testing on phantom dataset with k-space subsampling factor 70%. Comparison between BLIP [3], FLOR [6], CNN by Hoppe et al. [11], FNN by Cohen et al. [10] and proposed HYDRA. Note that, CNN [11], FNN [10] and MRF-ResNet uses low-rank based signature de-aliasing followed by network based parameter mapping. It is noticed that the proposed HYDRA outperforms dictionary matching methods, including state-of-the-art FLOR [6], as well as competing deep learning methods. (Zoom-in in a electric screen for better visualization)



(a) T1 Reference (left) and T2 Reference (right).



(b) T1 estimation (top row) and residual errors (bottom row).



(c) T2 estimation (top row) and residual errors (bottom row).

BLIP [3]	FLOR [6]	CNN [11]	FNN [10]	proposed HYDRA
SNR = 20.99 / 14.58 dB	SNR = 30.51 / 21.89 dB	SNR = 29.23 / 12.26 dB	SNR = 30.58 / 21.32 dB	SNR = 30.76 / 19.78 dB

Fig. 11. Visual results of testing on phantom dataset with k-space subsampling factor 15%. Comparison between BLIP [3], FLOR [6], CNN by Hoppe et al. [11], FNN by Cohen et al. [10] and proposed HYDRA. It is noticed that the advantage of deep learning methods over dictionary matching methods degrades for a higher subsampling factor. Because the restored signatures from highly subsampled k-space data exhibit stronger deviations from the groundtruth, thus leading to poorer input for the trained networks. (Zoom-in in a electric screen for better visualization)